



ACOUSTIC AND VIBRATION ANALYSIS OF AN ELECTRIC POWERTRAIN FOR PASSENGER CARS

S. T. Spanjer, s1481150

Bosch, Powertrain Solutions, Electromobility
Schwieberdingen, Germany, 04/18-08/18

R. Meikandan
A.de Boer

1. Summary

The eAxle is the modular electric powertrain solution for passenger cars from Bosch. The eAxle consists of an electromotor, power electronics and a gearbox. To make these eAxles competitive with other suppliers and to meet market demands high requirements on the noise radiation of the eAxle are set. To full fill these requirements in terms of structural vibrations and noise radiation, while maintaining low weight, high performance and cooling capacity, targeted measures should be taken to reduce the level of vibrations in the system.

In this report first several of the more dominant noise sources in eAxle like systems are discussed together with their frequency domain characteristics. In the second part of the report a set of measurements is described which could be used to identify and quantify the vibrations and noise radiation of the eAxle. Knowledge about the cause and the severity of the vibrations could be used to determine the most optimal measures that could be taken to meet the requirements.

Author: Sil T. Spanjer

Keywords: Structural acoustics, Vibration sources, Dynamics measurements, Electromotive

Contents

1. Summary	1
2. Introduction	5
3. Problem description	5
4. Bosch eAxle	6
5. Theoretical Background	7
5.1. Harmonic Orders	7
5.2. Campbell Diagram	8
5.3. Order Plot	9
5.3.1. Variable DFT size	10
5.3.2. RPM-sync resampling	10
5.3.3. Time domain averaging	11
5.4. E-Machine harmonics	11
5.4.1. One times rotational frequency	11
5.4.2. Rotor bar passing	11
5.4.3. Twice line frequency vibration	12
5.4.4. Rotor deflection due to fundamental flux	12
5.4.5. Rotor resonance frequencies	12
5.4.6. Pulse Width modulation frequencies	13
5.4.7. Failure related vibration sources	13
5.5. Bearing Harmonics	13
5.5.1. Fundamental bearing frequencies	14
5.5.2. Variable compliance	15
5.5.3. Geometric imperfections	15
5.5.4. Surface roughness	16
5.5.5. Waviness	16
5.5.6. Discrete effects	17
5.6. Gearbox Harmonics	17
5.7. Power Electronic Harmonics	18
5.8. Structural Harmonics	19
5.9. Modal assurance criterion	19
5.10. Acoustic radiation	20
5.11. Equal loudness curve	21
6. Types of Measurements	22
6.1. Structure Borne Noise measurements	22
6.1.1. Setup	22
6.1.2. Preparation	25
6.1.3. Measurement	26

6.1.4. Tips, tricks and other remarks	26
6.2. Air Borne Noise measurements	26
6.3. Experimental Modal Analysis	27
6.3.1. Hammer excitation	27
6.3.2. Shaker excitation	28
6.3.3. Measurement of the FRF	28
6.3.4. Modes	29
6.4. Operational Deflection Shape	29
7. Simulation	30
8. Conclusion	30
A. Window functions	31
A.1. Bartlet window	31
A.2. Hanning window	32
A.3. Hamming window	33
A.4. Blackman window	35
A.5. Flat top window	35
A.6. Gaussian window	37
A.7. Kaiser window	38
B. Reflection	38

List of Figures

1. Maximum noise level from different types of cars measured with pass-by measurements, from a French study by Joël Lelong and Roger Michelet, according to [1]	6
3. Campbell of 50Nm motoric ramp up.	8
4. Example of an order plot with 50Nm load on ramp up.	9
5. Schematic view of an induction motor.	11
6. Schematic view of a bearing.	14
7. Response rectangular plate, obtained from Xie et al. [2]	21
8. Equal loudness curves as defined in ISO 226:2003.	22
9. eAxle mounted on a testbench with hard mounts	23
10. eAxle torque curves for structure borne noise measurements.	24
11. Spatial grid for EMA	28
12. EMA setup with laser-vibrometers	29
13. Example modeshapes	30
14. Example of spectral leakage and scalloping loss with a rectangular window.	32
15. Bartlet function in time and frequency domain	33
16. Hanning window in Dirichlet kernels	34

17.	Hanning function in time and frequency domain	34
18.	Hamming function in time and frequency domain	35
19.	Blackman function in time and frequency domain	36
20.	Flattop function in time and frequency domain	37
21.	Gaussian function in time and frequency domain	38
22.	Kaiser function in time and frequency domain	39

2. Introduction

Robert Bosch GmbH, or Bosch for short, is a German multinational founded in Stuttgart in 1886 by Robert Bosch. Originally it was called the Workshop for Precision Mechanics and Electrical Engineering. The first success product by Bosch was the magneto ignition system. From the magneto ignition system the product line was expanded to all sorts of parts for the automotive industry like lamps, horns wipers and diesel injection pumps. The crisis in the German automotive industry in 1926 led to an expansion of the product portfolio into new areas like power tools, thermotechnology, radio and television. In the early 1950s Bosch entered the market of kitchen appliances. Bosch started developing electronic components in the mid-1950s, starting with the variode and the transistor a few years after that. From 1970 integrated circuits are being developed. In 1960 Bosch employed around 70000 employees. In 1990 development in micromechanical sensors started. Since 2000 several other fields have been taken up by Bosch, like the E-bike drives, healthcare and internet of things. At the moment Bosch has 409000 employees [3].

For my internship I went to the Robert Bosch company, area Stuttgart, location Schwieberdingen. During my internship I worked in the Powertrain Solutions department, branch Electro Mobility. Here I worked on the eAxle project. On the eAxle project worked around 150 people. On this project I worked in the Noise Vibration and Harshment (NVH) team, consisting of 5 people. The role I fulfilled there is doing several types of measurements and analysing the data gathered. A detailed description of the measurements can be found in section 6.

This report focusses on the description of a theoretical background to the sources of vibrations and methods to define noise limiting measures. The theory in this report is focussed on the application on the eAxle, but is also applicable in a wide range of other NVH design problems.

3. Problem description

The eAxle is a compact electric drive for electric and hybrid vehicles in which the electric motor, power electronics and transmission are combined into a compact unit[4]. This unit directly drives the wheels of the vehicle. The eAxle has several properties that are important for the use in passenger vehicles. These are for example weight, efficiency, size, durability, peak/continuous power and noise emission. The noise emission for this type of powertrain is relatively more important than for traditional internal combustion engines. In figure 1 a comparison between the pass-by noise of different powertrain types is displayed. As can be seen in the figure, the noise emission of electric powertrains is low especially on low speeds. This is caused by the lack of combustion in the engine and therefore reveals noise sources that are normally masked by the combustion noise or are typical for electric powertrains. Also, the expected noise levels for electric powertrains

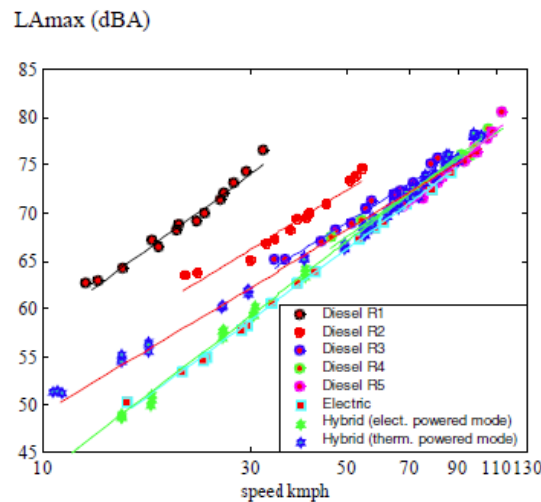


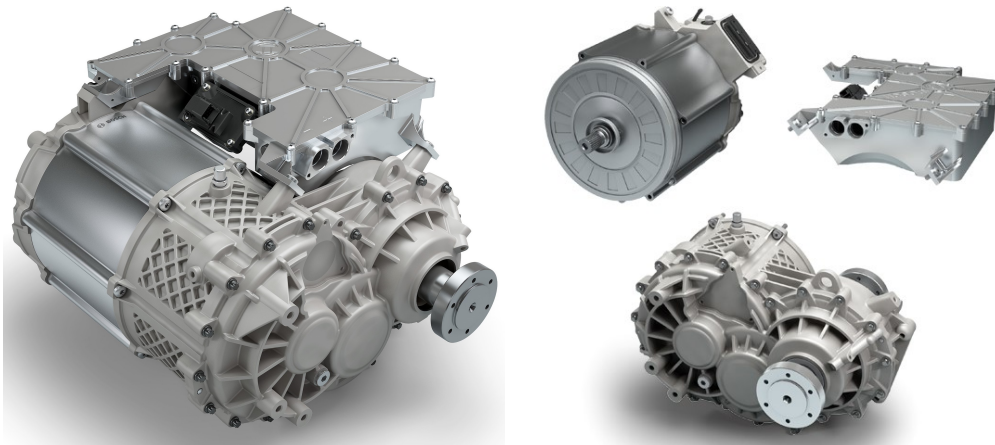
Figure 1: Maximum noise level from different types of cars measured with pass-by measurements, from a French study by Joël Lelong and Roger Michelet, according to [1]

are low.

To keep the noise levels of both air borne as well as structure borne noise under a predefined level while keeping the weight and size of the system down requires targeted measures to be taken. This report focusses on a theoretical investigation of the noise sources present in electric powertrains and the process to derive a set of measures to be implemented to improve the NVH behaviour of the powertrain.

4. Bosch eAxle

The main components of the eAxle are the electric motor, or EMachine, the power electronics and the transmission. An overview of the eAxle can be seen in 2a, the different parts are displayed in exploded view in figure 2b. The eAxle product line is a modular platform with a power range of 50-300kW. The torque of the eAxle ranges of 1000-6000Nm and the electric motor has a speed limit of 16000 RPM [4]. In this report no distinction will be made between the differently specced eAxles since the content applies to the complete range of possible eAxles. The gearbox is a two stage gear reduction box, the electric motor is a permanent magnet induction motor. The rotor is supported by two bearings. The bearing on the gearbox side is called the A-lager, the bearing on the other side is the B-lager. The housing of the eAxle is actively cooled by an external cooling loop.



(a) eAxle overview

(b) eAxle exploded view

5. Theoretical Background

For the analysis of the NVH behaviour of the eAxle a distinction is made between air borne and structure borne noise. As the name implies, the air borne noise are vibrations in the air and the structure borne noise are vibrations in the structure. Air borne noise is caused by the structure borne vibrations. An introduction to the concept of acoustic radiation is described in section 5.10.

In this section of the report first a couple of concepts and analysis tools are described. The second part of the theoretical background evaluates the different noise sources in electric vehicles.

5.1. Harmonic Orders

It is common practice to express the acoustic behaviour of a motor driven object in harmonic orders. These harmonic orders are scalar multiples of the rotation frequency of the driving shaft. The harmonic orders are indicated with the value of the scalar. This need not be an integer. Expressing the vibrational behaviour of a rotating system in terms of harmonic orders enables easy source identification of the noise that corresponds to the measured sound or vibration. The frequency in Hertz associated with a specific harmonic order and RPM can be found by:

$$f = n \cdot \frac{RPM}{60} \quad (1)$$

In which n is the harmonic order.

There are two commonly used methods to visualise the harmonic orders. The first is to display the data as a Campbell diagram, the second method is to make an orderplot. These two methods are discussed in section 5.2 and 5.3 respectively.

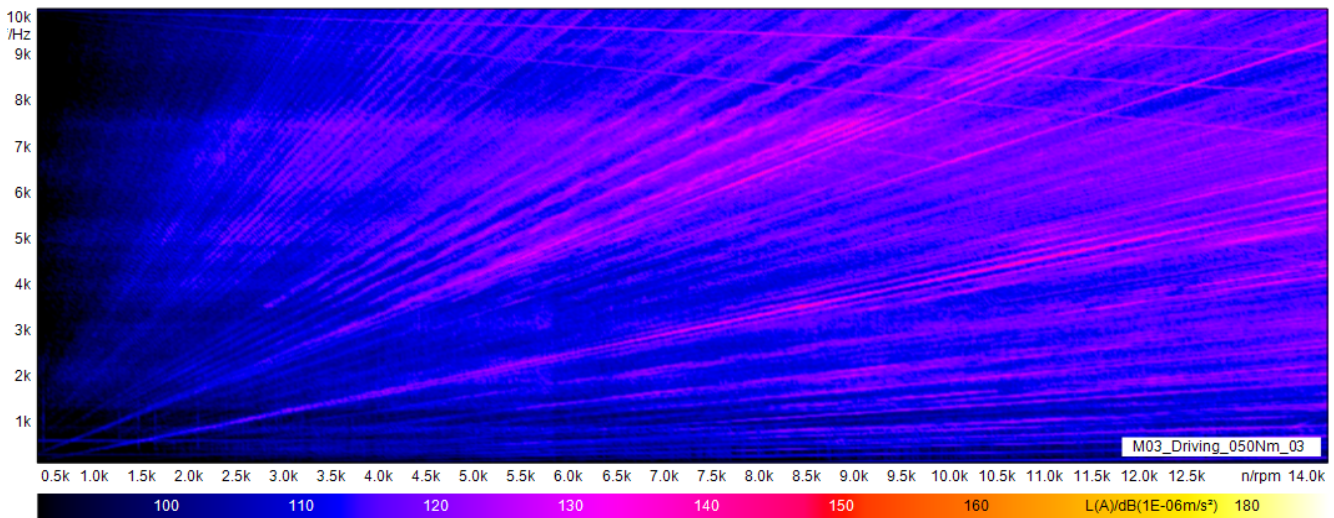


Figure 3: Campbell of 50Nm motoric ramp up.

5.2. Campbell Diagram

In a Campbell diagram the frequency response is plotted against the RPM. An example of a Campbell diagram is shown in figure 3.

The amplitude is plotted in the third dimension. The harmonic orders can be seen in a linearly scaled Campbell diagram as straight lines with an angle depending on the order. All the harmonic orders pass through the origin. Eigenfrequencies can be seen as horizontal lines in the response. Vertical lines in the response can have several causes but indicate discontinuities in the measurement. To make a Campbell diagram the data is first split in to windows with a predefined sample width. Typically this window has 2^n samples, with $n \geq 8$. A special window function is used to reduce the leaking in frequency domain typically associated with a rectangular window. A summary of common window functions is given in section A, but generally the Hanning window provides good overall performance and is commonly used. The windowed data is Fourier transformed to frequency domain and plotted in a vertical line in the Campbell diagram. The position on the x-axis is depending on the mean value of the RPM channel. The spectral and time resolution of the Campbell diagram is dependent on the sampling frequency (f_s) and the chunk size used for each Fourier transform. The upper bound is determined by the Nyquist frequency. The number of bins in the frequency interval is half of the number of samples (N). Combining this gives the spectral resolution of equation 2.

$$dF = \frac{f_s}{N} \quad (2)$$

The resolution on the RPM axis is predefined in the used software, but the lower bound, where all data is used and none of the samples are used double, is determined by the

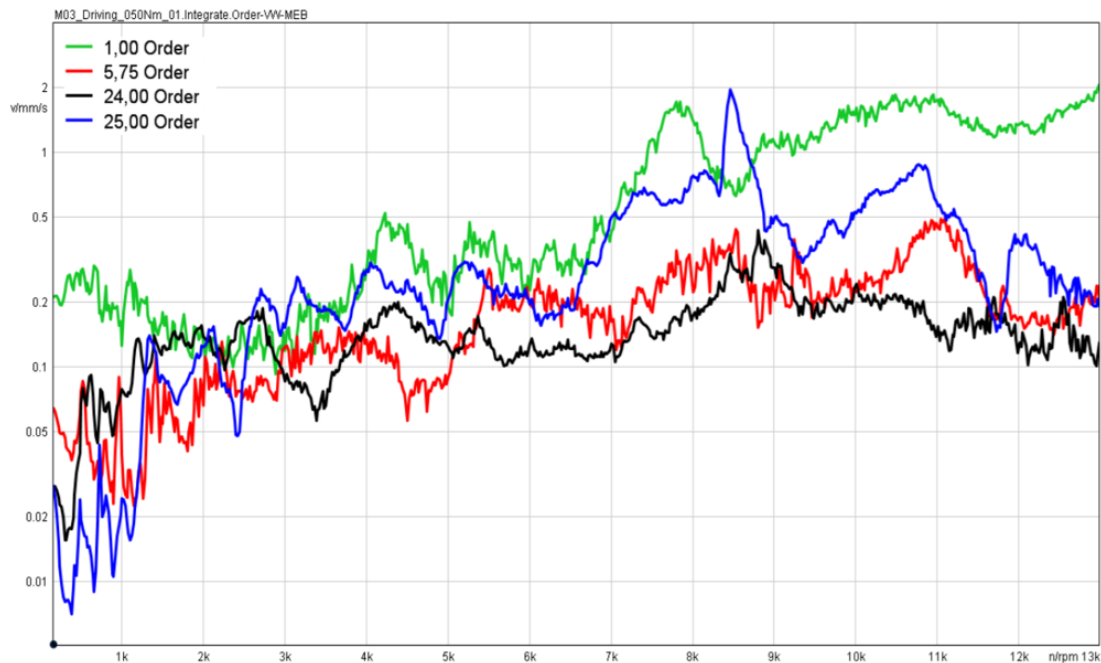


Figure 4: Example of an order plot with 50Nm load on ramp up.

chunk size, sampling frequency and the slew rate of the RPM signal. The slew rate v_{RPM} of the RPM signal is defined as the time derivative of the RPM signal. The RPM resolution is given in equation 3. A mismatch in minimal RPM resolution and requested resolution is solved by discarding data or overlapping the sample periods.

$$dRPM = \frac{N \cdot v_{rpm}}{f_s} \quad (3)$$

5.3. Order Plot

Although the Campbell diagram gives good insight in the overall vibrational behaviour of the system, it is less suited for detailed analysis of individual orders. For this reason order plots are used. The order plot essentially is a Campbell diagram that is cut through the origin in a specific angle. This angle is dependent on the required order. An example of an order plot can be seen in figure 4.

The values of the orderplot O_v can be extracted from the Campbell diagram via equation 4, but generally it is calculated separate with dedicated algorithms which either decrease the computational load and/or increase the accuracy. There are three algorithms available for the calculation of the order plots, these are: domain averaging, variable dft size and RMS-sync resampling. These algorithms are discussed in the sections 5.3.1 to 5.3.3.

$$O_v = Campbell(RPM, \frac{RPM}{60} \cdot Order) \quad (4)$$

5.3.1. Variable DFT size

Variable dft size uses the fact that the minimum required window width is inversely proportional to the rpm. This can be expressed as equation 5 in which the Δt is depending on the rpm.

$$\Delta t = \frac{60}{rpm \cdot OrderResolution} \quad (5)$$

The calculation procedure starts with defining the windows on the data based on the order resolution and the rpm values. A window function is applied and the Fourier transformed results are used to make the plots. The advantage of this method is that it is a fast way of calculating order plots. However, not all the measurement data is used. Also this method assumes that in the data window, the rpm signal does not change rapidly over time. RPM signals that change rapidly over time can occur smeared in the order plots. To overcome this downside the RPM-sync resampling method is used.

5.3.2. RPM-sync resampling

The variable DFT size method discussed in the previous section assumes that the rotational frequency does not change during the time window. For slow changes in RPM this is the case, but when sudden jumps in the RMP can be expected this is no longer valid. Also, according to equation 5 the time window increases in width when for low RPM making the allowed rate of change of the RPM lower then for high RPM. This effect can be seen in the Campbell diagram and the order plots as 'smearing' of the signal.

This can be solved by a method called RPM-sync resampling. For this method the measured signal is resampled to yield a rotational angle equidistant signal. The Fourier transform of this signal can be used to construct the order plot if the RPM values are known. In contrast to the variable dft size method, the resampling of the data results in the same number of samples for each sampling point. The downside of the RPM-sync resampling method is the high computational load, especially if high orders and are required.

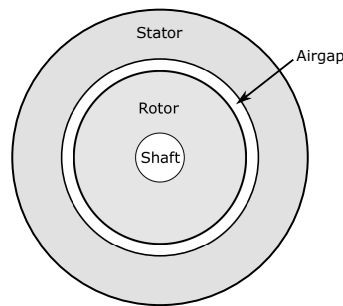


Figure 5: Schematic view of an induction motor.

5.3.3. Time domain averaging

This method is based on the RPM-sync resampled signal. In addition to the resampling, samples with identical phasing are averaged in time domain. Averaging in time domain reduces the measurement noise.

5.4. E-Machine harmonics

There are several sources of vibration present in an induction motor. In this section the individual sources are discussed. Consider for this section the model of the induction motor as given in figure 5. For a detailed description of the working principle, see [5].

5.4.1. One times rotational frequency

At one times the rotational frequency of the motor the vibration can be caused by either eccentricity of the rotor with respect to the stator, or an imbalance in the rotor or shaft. Eccentricity yields an air gap between the rotor and the stator that varies with the angle of the rotor and has a maximum and minimum width. The minimum air gap rotates with the rotor at one times the rotational frequency. Due to this misalignment there is a net unbalanced force component that causes vibrations.

An imbalance in the rotor or shaft leads to a vibration on the same frequency. In practise each rotor-shaft combination is individually balanced to minimize these effects.

5.4.2. Rotor bar passing

At the frequency at which the poles of the rotor pass the teeth of the stator, a vibration can be seen. This vibration is caused by the tangential forces from the rotor to the stator teeth. These forces cause a vibration due to the varying nature that depends on the distance between the rotor pole and the stator teeth. The rotor bar passing frequency of the motor is typically much higher than the other sources of vibration in the system.

Due to the high frequent nature of this source the displacements associated with the rotor bar passing are small [6]. The velocities of these vibrations however are significant and well in the audible range. For example, an electric motor with 3 phases and 8 poles has a rotor bar passing frequency F_{bp} equal to:

$$F_{bp} = n_{poles} \cdot n_{phases} \cdot f_{rot} \quad (6)$$

This yields a harmonic order of 24. This results for a rotational frequency of 5kRPM in a frequency of 2kHz.

5.4.3. Twice line frequency vibration

The power electronics provide a PWM based, sinusoidal shaped current to the motor. This current is used to create an electromagnetic force in the motor. This force is maximum when the amplitude of the current is maximal. This happens twice every current wave, one time when the current is maximal and one time when the current is minimal. The frequency of the current wave is the line frequency.

5.4.4. Rotor deflection due to fundamental flux

The electromechanical force in the rotor will attempt to deform the rotor. For a two pole motor, the fundamental flux deforms the rotor to an elliptical shape. The deflection is determined by the stiffness of the rotor and the applied fundamental flux. Also the number of poles is of major importance. Since the poles of a 4 pole motor are only 90 degree apart, the resulting deflection will be an order of magnitude lower then for the two pole variant with similar power characteristics[6].

5.4.5. Rotor resonance frequencies

The rotor can be seen as a beam that is supported in the stator assembly with one rotational degree of freedom. Since the size of the rotor is limited, the bending and torsion modes of the system can be in the operational range of the motor. If the resonance frequency is close to an excitation frequency, high vibrations can be expected. To find the resonance frequency of the rotor a first principles estimate can be made based on the Euler-Bernoulli beam equations for a two ends clamped situation. For transversal vibrations, this is given by:

$$\omega_n = n^2 \pi^2 \sqrt{\frac{EI}{\rho AL^4}} \quad (7)$$

In which n is n^{th} mode, E is the elastic modulus, I is the second moment of inertia, ρ is the density, A is the cross sectional area and L is the length of the beam.

For longitudinal vibrations this is:

$$\omega_n = n\pi\sqrt{\frac{E}{\rho L^2}} \quad (8)$$

And for torsion vibrations this is:

$$\omega_n = n\pi\sqrt{\frac{G}{L^2\rho}} \quad (9)$$

In which G is the shear modulus.

However, the Euler-Bernoulli equations assume that the cross-section of the beam does not change during loading. Also the used bearings do not have an infinite stiffness, and the permanent magnets in the rotor make the material non-homogeneous and anisotropic. These effects should be taken into account when considering the resonance frequencies. A FEM model that takes into account these effects can be used to determine the modes of the rotor.

5.4.6. Pulse Width modulation frequencies

In modern applications, electric motors are typically controlled with PWM signals. These signals cause vibrations in the electric motor. The characteristics of the vibrations are discussed in section 5.7.

5.4.7. Failure related vibration sources

There are several vibration sources that are related to failures in the electrical/mechanical system. These are not discussed here since they describe phenomena that are not important for the optimization of the NVH behaviour. Knowledge over these sources could be used to identify faults in the system while the system is running. For a description on these effects, the reader is referred to Finley et al. [6].

5.5. Bearing Harmonics

In the EMachine and the gearbox of the eAxle several bearings can be found. These bearings are the source of vibrations due to several causes and on different harmonic orders. In this section bearings with a stationary outer ring and rotating inner ring are considered. In figure 6 a schematic overview of a bearing is displayed. In this section first the fundamental frequencies of a properly working bearing are discussed, thereafter several causes of vibrations are discussed.

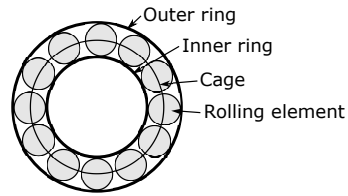


Figure 6: Schematic view of a bearing.

5.5.1. Fundamental bearing frequencies

The fundamental frequencies of a bearing are listed from equation 10 to 14[7].

$$f_{c/o} = f_r/2[1 - \frac{d}{D}\cos(a)] \quad (10)$$

$$f_{c/i} = f_r/2[1 + \frac{d}{D}\cos(a)] \quad (11)$$

$$f_{n/o} = Z \cdot f_{c/o} \quad (12)$$

$$f_{b/i} = Z \cdot f_{c/i} \quad (13)$$

$$f_b = D/2df_r \left[1 - \left(\frac{d}{D}\cos(\alpha) \right)^2 \right] \quad (14)$$

in which:

- f_r = inner ring rotational frequency.
- $f_{c/o}$ = fundamental cage frequency relative to the outer ring.
- $f_{c/i}$ = fundamental cage frequency relative to the inner ring.
- $f_{b/o}$ = ball pass frequency of outer ring.
- $f_{b/i}$ = ball pass frequency of inner ring.
- f_b = rolling element spin frequency.
- D = Pitch circle diameter.
- d = diameter of roller elements
- α = contact angle.

The pitch circle diameter is the diameter of the circle that passes through the centre of all rolling elements of the bearing. In the case that there is no distance between the rolling elements and the inner and outer ring, the pitch circle diameter is equal to the difference in radius of the inner and outer circle.

5.5.2. Variable compliance

Under radial loading bearing vibration is caused by the variable compliance due to the external load being supported by a discrete number of load bearing elements, even in geometrically perfect bearings. Rotation of these elements change the location and direction of the force vector applied by the load bearing elements on the inner as well as the outer ring. Variable compliance in a bearing decreases with an increase in the number of load bearing elements. Furthermore, a decrease in clearance reduces the variable compliance based vibrations. When ball bearings are used, this effect can be reduced to negligible levels when the correct pre-load is used [8]

5.5.3. Geometric imperfections

The manufacturing of bearings introduces geometrical imperfections in the bearings. These imperfections are of vary per bearing and are described with the tolerance class of the bearing, which are specified in ISO 492 and ISO 199 [9]. The ISO norms determine the accuracy of the bearings on different measures. These are:

- The range and variation of bore diameter and the deviation from its nominal size in any cross section.
- The range of inner ring width and the deviation from its nominal size in any cross section.
- The range and variation of the outer diameter and the deviation from its nominal size in any cross section.
- The range of the outer ring width and the deviation from its nominal size in any cross section.
- The circular run-out of the inner ring inner surface with respect to the outer ring outer surface.
- The circular run-out of the outer ring outside surface with respect to the inner ring bore surface.

It is convenient to make a distinction between geometric imperfections and surface roughness. All surface features with a wavelength in the same order or smaller than the contact length are grouped under surface roughness, all features with wavelengths larger than the contact length are grouped as geometric imperfections.

5.5.4. Surface roughness

Surface roughness can be a main source of vibration when the level of roughness is high in comparison to the thickness of the lubrication film. In this case, the peaks of the surface can break through the lubrication film and collide with the opposing surfaces. This results in random impulses that excite all vibration modes of the bearing. A common method of measuring the level of surface roughness with respect to the lubrication film thickness is the Λ ratio:

$$\Lambda = \frac{h}{\sqrt{\sigma_b^2 + \sigma_r^2}} \quad (15)$$

in which h is the lubrication film thickness, σ_b and σ_r are the RMS roughness of the ball and the raceway respectively. In literature, different guidelines can be found for the Λ ration, here the guideline from [10] is used.

- $\Lambda < 1$: Boundary lubrication. The surfaces are not separated by the lubrication film and the effects of the lubrication are negligible. This lubrication regime is characterized by high wear and high friction. The contact lubrication is governed by a thin surface film of molecular dimensions. Although the wear rate of unlubricated surfaces is much higher than for surfaces in the boundary lubrication regime, still the wear rate is too high for most applications, especially in automotive applications where high reliability and long lifetime need to be guaranteed.
- $1 \leq \Lambda < 5$: Partial lubrication. Mixed regime between boundary lubrication and hydrodynamic lubrication. Occasionally the lubrication film is pierced when the running speed is too low or the pressure in the fluid film too high.
- $5 \leq \Lambda$: Hydrodynamic lubrication, characterized by full separation between the rolling surfaces. Hydrodynamic lubrication is seen as the ideal form of lubrication since it has low friction and high resistance to wear.

The Λ ration is a rough estimate of the lubrication regime the bearing operates in. More detailed expressions can be derived for the minimum film thickness of a bearing to maintain the required lubrication regime. These expressions depend on for example the applied normal load, fluid velocity, lubrication viscosity and surface roughness. For more information see [10].

5.5.5. Waviness

The waviness of the raceway causes vibrations up to 300 times the rotational speed [7]. This upper bound is explained by the smoothing effect of the finite stiffness contact mechanics of short wave length features. Waviness cannot be eliminated from the bearing geometry due to limitations in machining technology.

5.5.6. Discrete effects

Discrete effects refer to damage in the bearings. These effects can be scratches, indentations, debris etc. This can be caused by poor mounting or maintenance, contamination or poor operating conditions. In the frequency spectrum of the bearing vibrations these effects are difficult to see, although the RMS vibration amplitude is several times as large as a normal bearing. In the time signal of the vibration of a bearing with discrete defects clear peaks can be identified, occurring at one of the characteristic frequencies of the bearing. These type of effects decrease the lifetime of a bearing and can be prevented by proper manufacturing and handling of the bearings in combination with a proper design that prevents debris from entering the bearing.

5.6. Gearbox Harmonics

There are various sources of vibration in gearbox systems. The main source is the fluctuation in Static Transmission Error (STE), [11]. The STE describes the difference between the actual position of the driven gear in comparison with the theoretical position and is defined by equation 16.

$$STE(\theta_1) = R_{b_j}\theta_2(\theta_1) - R_{b_1}\theta_1 \quad (16)$$

Where R_{b_j} is the radius of gear j . The difference between the actual and the theoretical position of the gear is mainly caused by geometrical deviations of the teeth, either voluntary as corrections or involuntary as defects, and of elastic deformations of the teeth under load. The fluctuation in the STE also causes a position dependent mesh stiffness. The fluctuations in the STE cause vibrations in the gears with a base frequency equal to the gear mesh frequency, which are transduced through the bearings to the gearbox housing. The deviations in the gear geometry can be caused by one or a combination of the following effects [12]:

- Thermal distortions
- Pinion distortion
- Gearcase deflection
- Gearcase accuracy
- Gear movement
- Tooth deflection
- Tooth profile accuracy
- Tooth pitch accuracy
- Tooth helix accuracy

To minimize the effects of the STE fluctuations, micro-geometrical modifications can be designed. Methods for fixed torque levels are well studied and an approach can be found in [13]. In this application a high spread of torque levels are to be expected, making the total number of solutions too large for FEM related solution methods due to the high computational load. A method to overcome this problem is proposed in [11].

To monitor the behaviour of the gearbox it is convenient to have a signal that averages a complete rotation of the input/output shaft and analyse the frequency spectrum of that signal. Averaging of the signal reduces the influences of noise where it comes at the cost of a longer measurement time. Also the time signal can be useful to identify defects in the gears, but it is more frequently used for fault diagnostics than for design purposes.

Another cause for vibrations in the system can be the eccentricity of the gears. This effect can be seen in the frequency analysis of the gearbox vibration by an increase in the sidebands around the gearmesh frequency. Characteristic of this phenomenon is that the sidebands are not symmetric. Also, misalignment of the gears can cause vibrations in the system. Typically, this can be seen in the frequency spectrum by a peak at the two times gear mesh frequency that is higher than the gear mesh frequency.

Another interesting phenomenon that can be seen in the frequency spectrum is the hunting tooth. The hunting tooth indicates a problem related to a specific set of teeth and occurs at the frequency those teeth meet, therefore this effect is mainly low frequent. A hunting tooth effect can be caused by i.e. scratches on teeth that collide during operation.

5.7. Power Electronic Harmonics

The power electronics are a vital part of the eAxle structure and provide the driving current for the motor. The current is regulated with an inverter that produces a PWM shaped voltage signal. The duty cycle of the PWM signal is dependent on the required torque and is determined with a carrier wave. The PWM signal contributes to the acoustic response of the signal with a high pitched noise. The exact description of the noise varies with the applied sampling modulation technique. For a detailed overview in the different sampling techniques, the reader is referred to [14]. The general harmonic form of the signal can be expressed as equation 17 [14].

$$F(t) = \sum_{n=1}^{\infty} \{C_0 \cos(n[\omega_0 t + \theta_0])\} + \sum_{m=1}^{\infty} \{C_0 \cos(m[\omega_c t + \theta_c])\} + \sum_{m=1}^{\infty} \sum_{n=-\infty}^{\infty} \{C_{mn} \cos(m[\omega_c t + \theta_c] + n[\omega_0 t + \theta_0])\} \quad (17)$$

Where ω_0 and θ_0 are the fundamental frequency and phase of the PWM signal respectively. ω_c and θ_c are the frequency and the phase of the carrier frequency. The first term of

equation 17 is the fundamental part of the frequency spectrum, the second part is the carrier frequency harmonics and the third part is the carrier wave sidebands. Since the fundamental frequency is directly related to the rotation speed of the motor, also the sideband frequencies depend on the rotation speed of the motor. Rewriting the frequency dependent part of the carrier wave sidebands yields equation 18.

$$\omega_{eff} = m\omega_c + n\omega_0 \quad (18)$$

This can be seen in figure 3. The carrier frequency of the PWM signal is 10kHz. The data is only plotted to 10kHz so only the sidebands in the range $m = 1$ and $n \in \mathbb{N} \setminus \{-\infty \leq m \leq 0\}$. Typically the amplitude of the sidebands decreases for higher $|m|$ [15], therefore only the first few sidebands are distinguishable in the figure.

5.8. Structural Harmonics

The vibrational behaviour of any structure can be seen as a summation of mode shapes and their corresponding eigenfrequencies. Depending on the excitation frequency and orientation of the structure the different modeshapes are excited. information about the shape and frequency of the mode shapes can give insight to vibrational problems that occur.

There are several ways to determine the modes structures. In section 6.3 the experimental modal analysis is described, in section 7 a simulation based method is introduced.

5.9. Modal assurance criterion

To match modes obtained from different measurements the modal assurance criterion can be used. For example, the operational deflection shape analysis, section 6.4 gives a set of modes that are excited with their amplitude and frequency at a specific operating point. Matching these modes with the modes found with the experimental modal analysis 6.3 can help to find the root cause of a vibration.

The original modal assurance criterion is defined as [16]:

$$MAC_{cdr} = \frac{|\psi_{cr}^T \psi_{dr}^*|^2}{\psi_{cr}^T \psi_{cr}^* \psi_{dr}^T \psi_{dr}^*} \quad (19)$$

In which ψ_{cr} is the modal vector, measured from source c for mode r , and ψ_{dr} the modal vector measured from the source d and mode r . The * denotes the complex conjugate. The MAC is a scalar constant that relates the degree of linearity between different modal vectors.

Equation 19 can be rewritten as:

$$MAC_{cdr} = \frac{\psi_{cr}^T \psi_{dr}^* \cdot \psi_{cr}^T \psi_{dr}^*}{\psi_{cr}^T \psi_{cr}^* \cdot \psi_{dr}^T \psi_{dr}^*} = MSF_{dcr} MSF_{cdr} \quad (20)$$

In which:

$$MSF_{cdr} = \frac{\psi_{cr}^T \psi_{dr}^*}{\psi_{dr}^T \psi_{dr}^*} \quad (21)$$

The MSF compares modal vector ψ_{cr} to the reference ψ_{dr} and returns a normalised complex scalar. Consider that each modal vector ψ_{cr} can be written as:

$$\psi_{cr} = \psi_{cr}^d + \psi_{cr}^n \quad (22)$$

Here ψ_{cr}^d is the part of the vector that correlates to ψ_{dr} and ψ_{cr}^n is the residual and considered to be noise. If the noise part of the modal vector is zero, the MSF value reduces to the euclidean length of ψ_{cr} normalised by the euclidean length of ψ_{dr} . If the correlated part is zero, the MSF reduces to zero. The extension to the MAC criterion provides a scalar real valued constant which ranges from zero to one. Note that the MAC only takes into account the mode shapes, the frequencies of the modes are not taken into account.

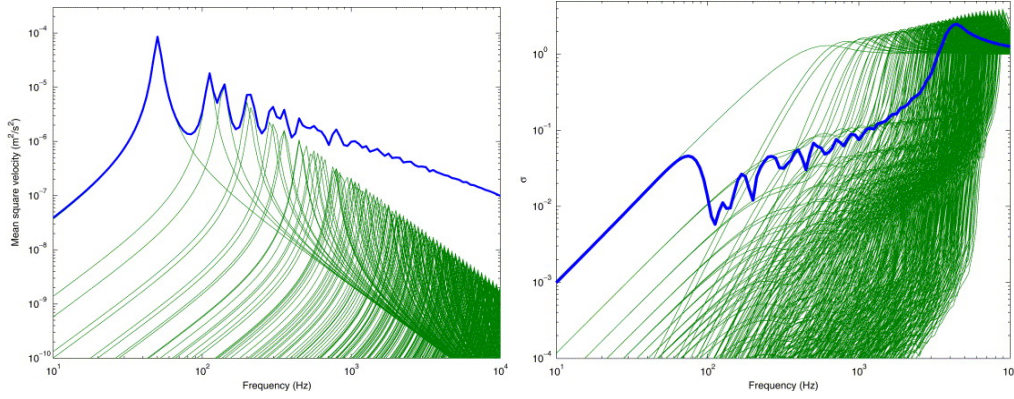
5.10. Acoustic radiation

The acoustic radiation of a structure like the eAxle is very complex to derive analytically and can only be approximated with the use of multi-physics finite element software packages like Abaqus and Comsol. To give a general idea of the principle, here the simple example of the infinite plate will be taken into consideration. For more details about the infinite plate and other examples is referred to Cremer et al. [17] and Xie et al. [2].

As discussed in section 5.8, the vibrations of a structure, or in this case a plate, can be seen as a summation of mode shapes. Each of these mode shapes has a corresponding radiation efficiency, usually called modal radiation efficiency, and is described by:

$$\sigma = \frac{W_{rad}}{\rho c S \langle v^2 \rangle} \quad (23)$$

where W_{rad} is the radiated power by the plate, $\langle v^2 \rangle$ is the average mean square normal velocity of the plate, S is the area of the plate and ρ and c are the air density and the speed of sound in air respectively [2]. The total acoustic radiation can also be described as a summation of modes [2].



(a) Average mean square velocity and modal contributions of a rectangular plate. (b) Average and modal radiation efficiencies of a rectangular plate.

Figure 7: Response rectangular plate, obtained from Xie et al. [2]

The total radiated acoustic power can be obtained by integrating the intensity of the far field acoustic intensity over a hemisphere of radius r :

$$W = \int_0^{2\pi} \int_0^{\frac{\pi}{2}} \frac{|p(\mathbf{r})|^2}{2\rho c} \mathbf{r}^2 \sin(\theta) d\theta d\phi \quad (24)$$

Here $p(r)$ is the complex acoustic pressure. The integral is described in spherical coordinates θ and ϕ . Using the Rayleigh integral the acoustic pressure on an infinite plate can be described [18]:

$$p(\mathbf{r}) = \frac{jk\rho c}{2\pi} \int_s v(\mathbf{x}) \frac{e^{-jk\mathbf{r}'}}{\mathbf{r}'} dx \quad (25)$$

in which $\mathbf{r}' = |\mathbf{r} - \mathbf{x}|$, k is the acoustic wave number. The surface velocity can be described as a summation of modeshapes according to:

$$v(\mathbf{x}) = \sum_{m=1}^{\infty} \sum_{n=1}^{\infty} u_{mn} \sin\left(\frac{m\pi x}{a}\right) \sin\left(\frac{n\pi y}{b}\right) \quad (26)$$

Here m and n are mode indices and a and b are some constants.

The results of this analysis can be found in figure 7. It can be seen that the radiation efficiency for the differs largely over the frequency range, this means that some modeshapes can have much higher excitation velocities than other modeshapes.

5.11. Equal loudness curve

Human hearing does not perceive tones with constant sound pressure level (SPL) but varying frequency as equally loud. This effect is described by the equal loudness curve and

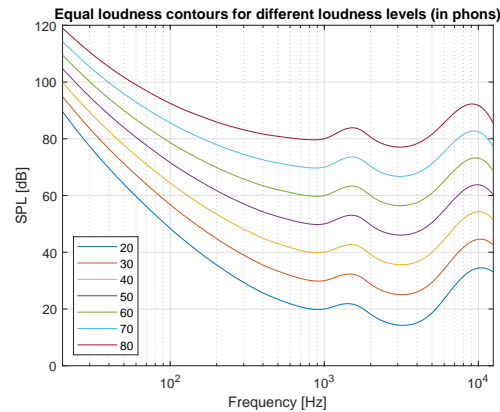


Figure 8: Equal loudness curves as defined in ISO 226:2003.

is defined in ISO norm 226:2003. The unit for perceived loudness of a specific frequency is described in *phon*. In figure 8 several equal loudness curves can be seen.

For air borne noise, it is common to weigh the results with the A-weighting filter. This scales the input according to the equal loudness curves.

6. Types of Measurements

In the previous sections common sources of vibration are discussed. To determine the performance of the eAxle and identify possible problems and improvement measures, several measurements can be done. In this section several of those measurements are discussed.

6.1. Structure Borne Noise measurements

6.1.1. Setup

The goal of the structural noise measurements is to measure the acceleration of the relevant surfaces during different load cycles. Which surfaces are relevant can be determined based on previous measurements and a general idea of the sources of vibration in the system. For this goal an eAxle is mounted on a test bench. The test bench consist of two electric motors, commonly referred to as braking machines, that, when combined can generate more torque and power than the eAxle itself over the entire RPM range. The eAxle can be mounted either rigidly or flexibly on the test bench which gives a different frequency response and surface characteristics. The complete setup can be mounted in a climate chamber. In figure 9 an eAxle mounted on a testbench can be seen.

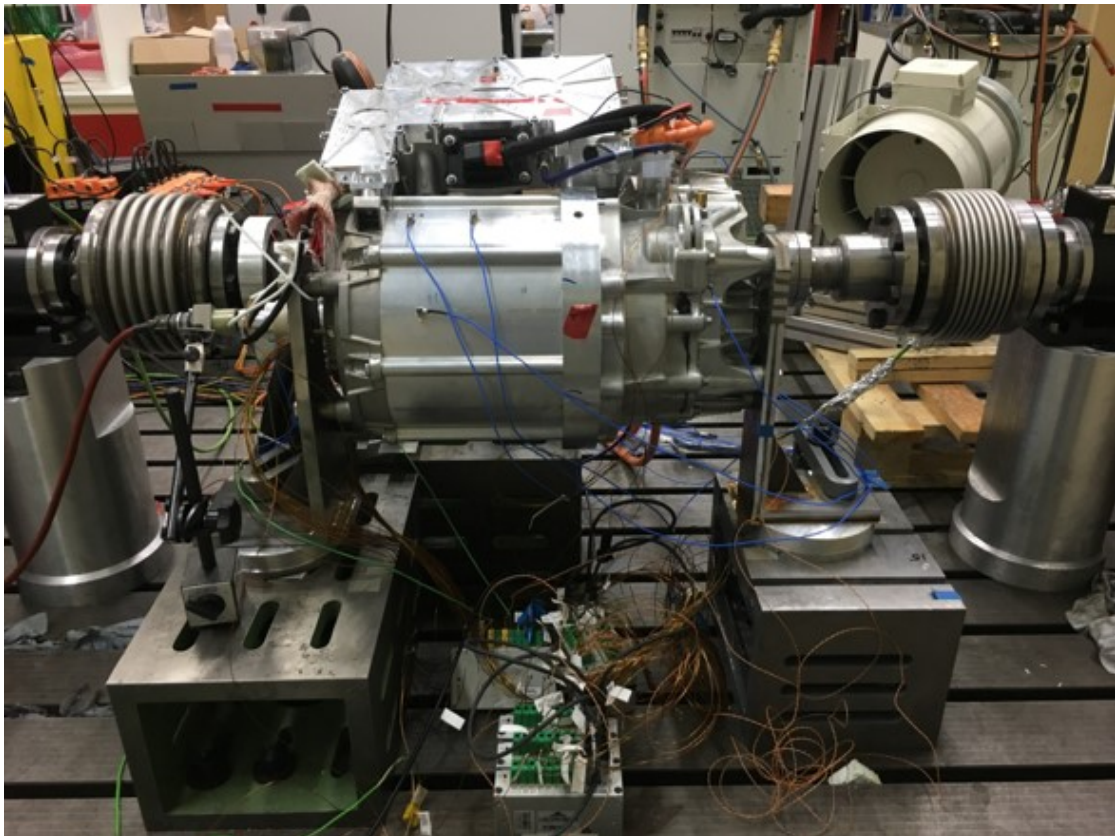


Figure 9: eAxle mounted on a testbench with hard mounts

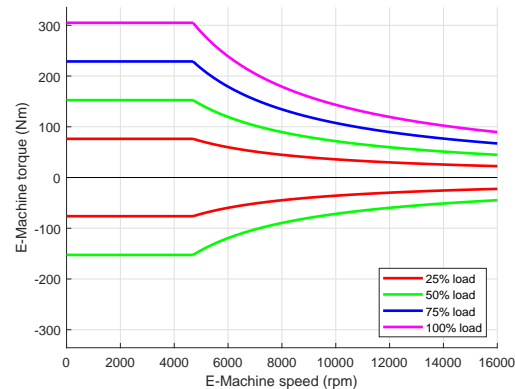


Figure 10: eAxe torque curves for structure borne noise measurements.

The braking machines have different control strategies to provide a wide variety of load cases. For the structure borne noise measurements, torque control is used. Torque control means that if the eAxe follows a specified torque profile, the torque of the braking machines is the changing parameter to match the revolution speed to the requirements. In figure 10 typical torque curves are displayed for an eAxe. These curves are defined as a percentage of the maximal power at each RPM. The flat part of the curves is the torque limitation, the curved part is the power limitation. In addition to the torque curves the slew rate of the eAxe needs to be defined to generate a complete time domain reference path.

The measurements can be performed with different temperatures. Typically coolant temperatures of 20°C and 60°C are used to approximate usual driving conditions in which the 20°C is the temperature at startup and 60°C the temperature during prolonged drive. The surface vibrations of the eAxe can change significantly with the changing temperature. To measure the surface accelerations, tri-axial accelerometers are used. The sensors are glued to aluminium mounting plates which have an electrically resistive coating on the mounting surface to isolate the sensors from electrical disturbances of the sample. The sensors together with the mounting plates are glued to the sample on specified positions. The position of the sensors is kept similar across different samples to be able to compare the results of different measurements and is based on previous measurements in which the interesting areas are defined. The numbering of these sensors is based on their position and is divided into 5 groups, the 100, 200, 300, 1000 and 2000 series. The global position of the groups is: e-machine, power-electronics, gearbox, mounting points and b-lager shield, respectively.

The b-lager shield is the cover of the bearing that supports the side of the EMachine that is not connected to the gearbox.

We performed mainly measurements with two different sensor setups, from here on

referred to as the extensive and the End Of Line (EOL) setup. The extensive setup uses 15 tri-axial sensors and 2 microphones. The EOL setup is based on the setup that is mainly used for testing at the manufacturing facility. It consists of only two tri-axial sensors of which only the z-direction is used. Each eAxle that is manufactured is measured on two points for the structure borne vibration performance. Spring loaded tips that measure the displacement are used in this application due to the quick and automatic application possibility. These sensors can only measure vibrations normal to the surface and are not suitable for high frequent measurements.

To record the accelerations from the sensors a head-acoustics front end is used. The head-acoustics front end is a modular setup which consist of one power, one data transmission and multiple data collection modules. The data transmission module can handle up to 48 channels. This means that for the extensive setup there is only one channel left. The setup can be extended with more data transmission modules if more than 48 channels are required. The power module uses an uninterruptible power supply principle and can support up to 2 data transmission modules. The data collection modules do not need separate power.

The data transmission module sends the collected data over an ethernet or USB cable to a laptop running recording software. The software used here is called ARTEMIS, also made by head-acoustics. The used accelerometers are of type HT356B01 of PCB piezotronics. The specifications are summarized by:

- Sensitivity: $0.51\text{mV} / (\text{m}/\text{s}^2) \pm 20\%$.
- Broadband resolution 1-10000Hz: $0.03\text{m}/\text{s}^2$ rms.
- Frequency range: 2-8000Hz.
- Temperature range: -54°C - 180°C .

The connector on the frontend is a D-sub 25 pin. Connected to this is an adapter which splits the cable from the connector to 6 bnc cable, each represent one channel. For the tri-axial sensors another adapter is used which converts three channels into a proprietary connector for the sensors.

Together with the tri-axial sensors and the microphones, also a CAN signal is recorded containing various system properties of the testbench. The characteristics of the eAxle, like the thermal behaviour, are recorded by a separate data logger. The property most interesting for this analysis is the RPM value of the braking machines. The glue used for the measurements is MD-405+ glue.

6.1.2. Preparation

To do a measurement, several steps should be taken. The first step is to glue the sensors to the surface of the sample on the required positions and connect the cables to the front end. In parallel with this process a list should be made which summarizes the sensor

serial numbers on the channels in the front end. This is important since each of the sensors has a slightly different calibrated value for the sensitivity which should be taken into account when recording the data. Also, it is essential to know which location the signal is coming from and how that signal is oriented in global coordinates.

This list is the input for the frontend and is required for a proper functioning of the system. To read the CAN signal a test bench specific .dbc file should be present to interpret the data from the CAN bus.

The load cycles to be measured should be specified in terms of torque and RPM. The test bench operators generally need to translate this to a series of setpoints in time from which the test bench software linearly interpolates the curve.

6.1.3. Measurement

The measurement can be started if all the preparations are complete and the temperature is within the specified range. After each load cycle the temperature should be dropped to the specified temperature. A 5 degrees difference is used between the stator temperature and the coolant to prevent excessive waiting times. Each measurement can be started if the difference is less or equal to this limit. Changing the setup from high to low temperature takes around 20 minutes.

6.1.4. Tips, tricks and other remarks

Due to the large number of cables required for an extensive setup, it is important to pay attention to the cable management in order to prevent mistakes which might be hard to identify and correct for. When a setup is frequently used, labelling the individual cables can save a lot of time in repetitive builds.

Removing the mounting plates from the sample is easiest with a wrench 9. With this tool there is the least risk of removing the mounting plate from the sensor or damaging one of the two. When little space is available a wide flat head screwdriver can be used.

6.2. Air Borne Noise measurements

The measurement of structure borne noise gives information about the vibrations of the eAxle, however, this cannot be translated directly to the air borne noise since the different modeshapes of structures have different radiating efficiencies [19]. To identify the airborne noise measurements, specific setups need to be used. The conditions for the airborne noise measurements are described in ISO norm 1680:2013. To perform airborne noise measurements it is required to isolate the sound emitted by the eAxle from the sound that has different sources like the braking machines and wall reflections. This can be done by performing the measurement in an anechoic chamber where the braking

machines are kept outside of the acoustic isolation.

Inside the anechoic chamber the tests performed are similar to the structure borne noise measurements in terms of load cases and operating conditions. Mostly also the structure borne noise is measured in parallel. Around the eAxle calibrated microphones are placed at predefined positions according to for example ISO 1680:2013. The output of the microphones is also recorded by the HEAD data recording module, taking up one channel per microphone.

The NVH requirements are mostly specified by a combination of a maximum air borne and structure borne noise level curve. To improve the airborne noise of the eAxle two strategies can be used, namely taking measures to decrease the structure borne noise levels and therefore also reducing the radiation of the eAxle, or implementing dampening covers on the eAxle.

6.3. Experimental Modal Analysis

As discussed in section 5.8 the motion of a structure can be described as a summation of modeshapes and their corresponding eigenfrequencies. Therefore knowledge about the modes of the structure can help to design effective measures to decrease the vibration levels. Modes of the structure refer to the modeshapes and corresponding eigenfrequencies of the system. An experimental modal analysis (EMA) can be done to identify the modes of the structure.

A continuous structure has an infinite number of modes which contribute to the total structural vibration. From an experimental point of view however, it is impossible to measure all those modes. For the EMA, the structure is sampled on a spatial grid. An example of such a spatial grid can be seen in figure 11. The spatial sampling determines the level of detail that can be incorporated in the identified modeshapes. However, the time required for the experimental part of the EMA scales linearly with the number of spatial samples.

From each of the spatial samples the frequency response function (FRF) needs to be determined. The FRF describes the input-output relation in frequency domain. The input of the measurement can be generated by either a hammer or a shaker. It is common to measure the FRF in free-free conditions. This can be done by suspending the eAxle in the air by an elastic rope or placing it on dampening mats. This is however not a requirement for the EMA.

6.3.1. Hammer excitation

Ideally a hammer approximates an impulse excitation. The frequency content of an impulse is constant over the complete spectrum. In reality however there are significant differences between the impulse frequency content and the frequency content provided by a hammer impact. This difference can be tuned to optimize the energy level in the relevant frequency range. For example, the impact hammer can be equipped with

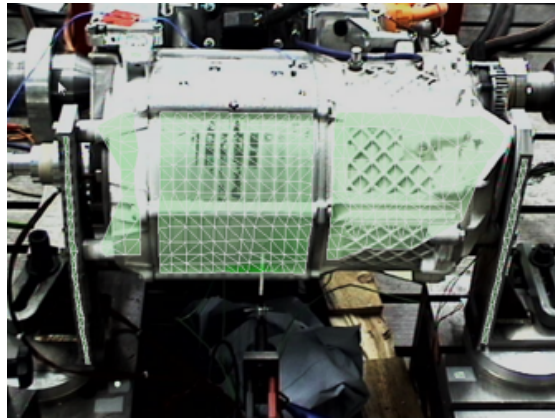


Figure 11: Spatial grid for EMA

different tips, ranging from soft to hard. Soft tips on the hammer are suitable for low frequency measurements while hard tips are better suited for high frequent measurements while having poorer performance in the low frequent range. Also, additional weights can be added to the hammer to provide extra energy to the system. The hammer needs to transfer enough energy to the structure to generate a measurable output at the measurement point, while too much energy excites non-linearities in the system. The hammer is equipped with a load cell to measure the input to the system.

6.3.2. Shaker excitation

A shaker can be used when the structure that needs to be measured is not suitable for hammer excitation. This can be the case for i.e. thin surfaces. To guarantee a consistent direction in which the force is applied, the shaker is commonly attached to the structure with a slender rod [20]. Different input signals can be used for the shaker, including white noise, binary white noise, multi sines and sweep sines. For a detailed discussion about input signals is referred to L.Ljung [21]. The rod is equipped with a load cell to measure the input to the system.

6.3.3. Measurement of the FRF

The output of the system is commonly measured with an accelerometer, either one-axial or tri-axial. An alternative for this is the use of laser-vibrometers. These laser based sensors use the Doppler effect to measure the surface velocity without the need to have physical contact with the eAxle. Using 3 laser heads enables 3D orthogonal decomposition of the signal. In the rest of this section we will use the hammer impact excitation. To measure the FRF on a spatially sampled grid on the eAxle, two methods are commonly used. These are roving hammer and the roving accelerometer method. The roving hammer



Figure 12: EMA setup with laser-vibrometers

method is most commonly used [20]. In this method the accelerometer is fixed in place and the hammer is used to excite the structure on different points along the spatial grid. The roving accelerometer method assumes a hammer impact location that is fixed in place and an accelerometer that is moved along the spatial grid. This method is cumbersome when accelerometers are used since gluing and removing of the accelerometers is time consuming. However, when laser-vibrometers are used this is the preferred method while the laserheads can move their focus point rapidly. The use of laser heads results in a setup as given in figure 12. It is common to measure the FRF multiple times and average the results.

6.3.4. Modes

When the FRF's are measured they can be used to determine the modes of the system. In figure 13 three examples are displayed of how these modes look like.

6.4. Operational Deflection Shape

Operational deflection shape analysis (ODS) is a similar technique to the EMA, however, where EMA is used to identify the natural vibration modes with the help of impact testing, the ODS uses its own operational forces as excitation source for the vibration. The benefit of this method is that also the interaction between the different noise sources

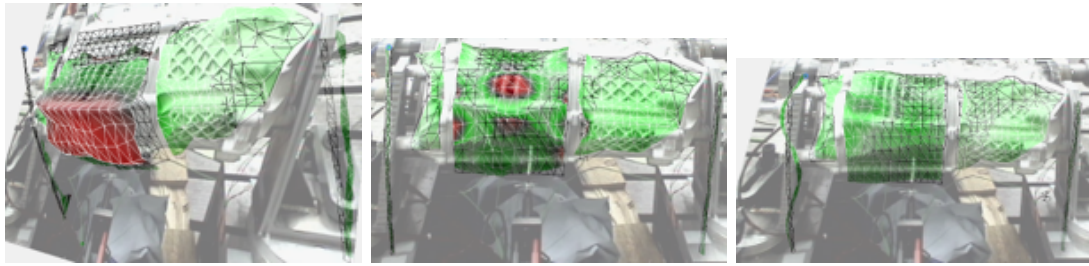


Figure 13: Example modeshapes

like the gear meshing and the structural vibration can be identified.

To perform an ODS on an eAxle, specific operating points need to be defined where the vibration characteristics are of interest. These points can be determined based on a structure borne noise measurement where the specific operating points match with peaks in the structure borne noise measurement.

The operational deflection shape can be compared to the natural mode shapes determined with the EMA.

7. Simulation

The simulation of systems plays an ever increasing role in the design process due to improvements in software and increasing availability of computational power. Simulation enables fast evaluation of system performance and quick validation of the effects of design changes. Due to the extensiveness of the subject and the availability of excellent literature on this subject there is no elaboration on this subject here. For further reading see i.e. Cook et al. [22]

8. Conclusion

In this report a comprehensive guide for NVH analysis of rotating electric machines is presented. Several theories about the root cause of vibrations are provided, in combination with descriptions of experiments to validate the performance in terms of vibrational behaviour.

A. Window functions

Section 5.2 discusses that a window function needs to be used to split the data in usable parts of finite length. This procedure is called windowing of the data and has an effect on the harmonic analysis of the data. The main effect induced by windowing the data is called spectral leakage. Spectral leakage is the effect that when a finite time interval is selected from an infinite set, and this interval is spectrally analysed, only frequencies that coincide with the basic set will project onto a single basis vector. All other frequencies have non-zero projections on the entire basis set. The basic vector set consists of harmonic waves with frequencies equal to multiples of $\frac{f_s}{N}$, in which N is the number of samples and f_s the sampling frequency. This can be explained by the fact that frequencies other than those of the basis set are non-periodic in the window [23]. Another effect is the scalloping loss. Scalloping loss is the difference between the actual amplitude of a harmonic wave in an infinite set and the measured amplitude from the finite set. The effect can be seen in figure 14. The figure displays the Discrete Fourier Transforms (DFT) of two harmonic signals of equal amplitude. One of the signals has a frequency which is an integer multiple of $\frac{f_s}{N}$, the second signal is shifted with $f_{shift} = 0.5 * \frac{f_s}{N}$. The integer multiple has an amplitude which is zero over the entire frequency domain except for the bin that equals its frequency. The small values can be explained by the floating point accuracy of MATLAB which is $\epsilon = 2.2204 \cdot 10^{-16}$. It can also be seen that the maximum amplitude of the shifted wave has decreased to only 63.7% of the non-shifted variant. Note that a rectangular window is used for these figures.

Several different window functions can be found in literature. In the following sections the most common window functions are described which are also supported by ARTEMIS suite.

The default setting for window functions of ARTEMIS suite is the Hanning window. This window is described in section A.2. This window function provides a good balance between scalloping loss and resolution, combined with a simple formulation.

A.1. Bartlet window

The Bartlet window, also called the triangular window, is one of the B-spline windows and can be seen in figure 15. The B-spline windows can be obtained as the k -fold convolution of the rectangular window. For the triangular window $k = 2$. The function can be described with equation 27. The width of the main lobe is approximately twice that of the rectangular window and the side lobes have a magnitude which is 26dB lower than the main lobe.[23].

$$w(n) = 1 - \left| \frac{n - \frac{N-1}{2}}{\frac{N}{2}} \right| \quad (27)$$

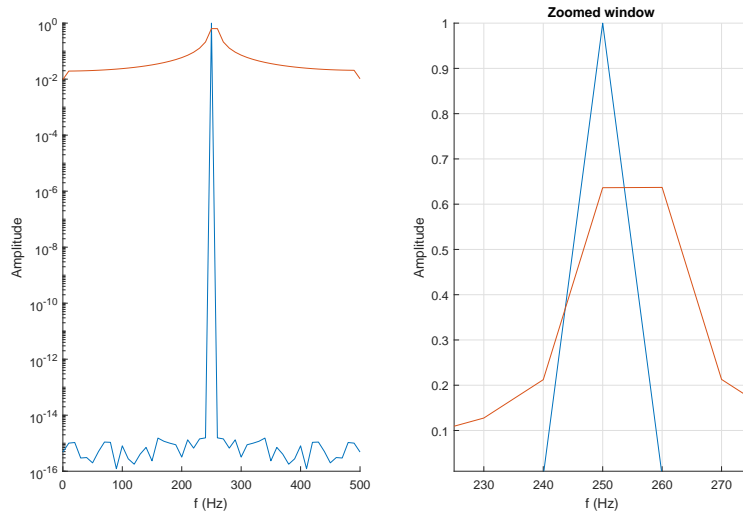


Figure 14: Example of spectral leakage and scalloping loss with a rectangular window.

Where N is the total number of samples.

A.2. Hanning window

The Hanning window is the first of the window functions of the \cos^α windows. This family of functions can be described by equation 28 [23].

$$w(n) = \cos^\alpha \left[\frac{n}{N} \pi \right], \quad n = \frac{-N}{2}, \dots, -1, 0, 1, \dots, \frac{N}{2} \quad (28)$$

The Hanning window uses $\alpha = 2$. The main advantage of this window is that not only the window itself is continuous, also its first derivative is continuous. The window can be described by 29[23] and be seen in figure 17.

$$w(n) = 0.5 + 0.5 \cos \left[\frac{2n}{N} \pi \right], \quad n = \frac{-N}{2}, \dots, -1, 0, 1, \dots, \frac{N}{2} \quad (29)$$

The DFT of the Hanning window can be described in terms of Dirichlet kernels as equation 30.

$$W(\theta) = 0.5D(\theta) + 0.25 \left[D \left(\theta - \frac{2\pi}{N} \right) + D \left(\theta + \frac{2\pi}{N} \right) \right] \quad (30)$$

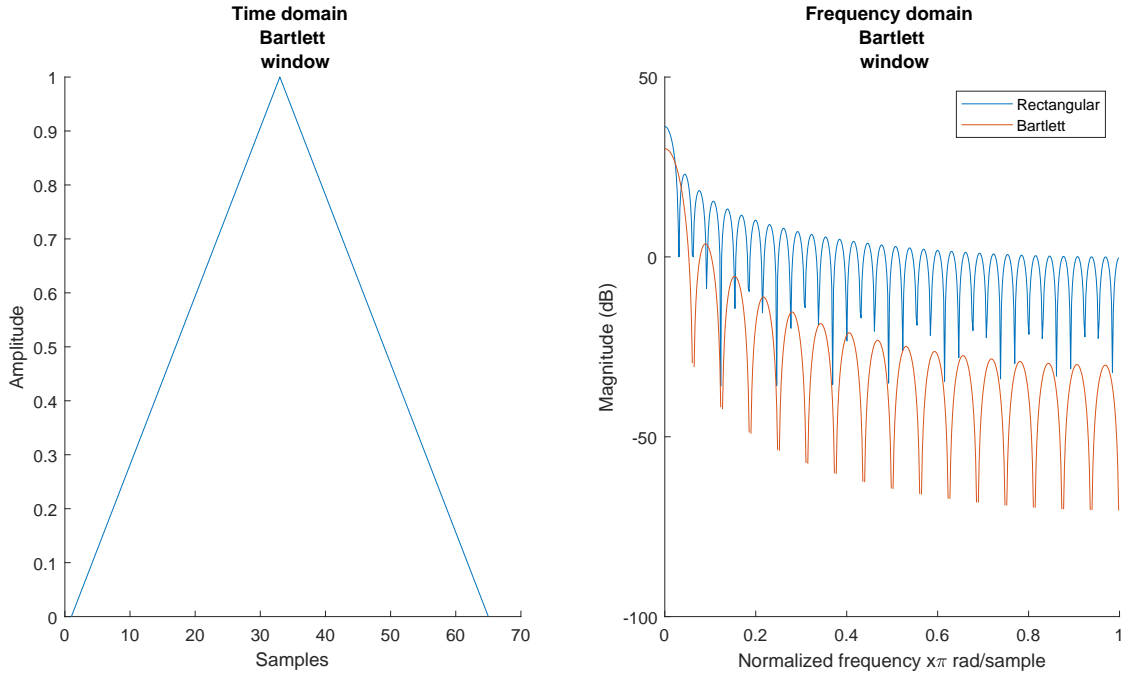


Figure 15: Bartlett function in time and frequency domain

with

$$D(\theta) = e^{\frac{\theta}{2}i} \frac{\sin\left(\frac{N}{2}\theta\right)}{\sin\left(\frac{1}{2}\theta\right)} \quad (31)$$

In equation 30 it can be recognised that the DFT of the Hanning window consist of three kernels. The main or centre kernel is centred on $\theta = 0$. The translated kernels are of half the size of the centre kernel and are translated with $\pm \frac{2\pi}{N}$. The translated kernels tend to cancel the sidelobe structure of the centre kernel. This can be seen in figure 16. Note that the side lobes are not exactly cancelled.

A.3. Hamming window

The Hamming window is a modified version of the Hanning window which adjusts the relative size of the kernels to maximise the cancellation of the side lobes [23]. This is described in equation 32 and in terms of Dirichlet kernels in equation 33.

$$w(n) = \alpha + (1 - \alpha) \cos\left[\frac{2n}{N}\pi\right], \quad n = \frac{-N}{2}, \dots, -1, 0, 1, \dots, \frac{N}{2} \quad (32)$$

$$W(\theta) = \alpha D(\theta) + 0.5(1 - \alpha) \left[D\left(\theta - \frac{2\pi}{N}\right) + D\left(\theta + \frac{2\pi}{N}\right) \right] \quad (33)$$

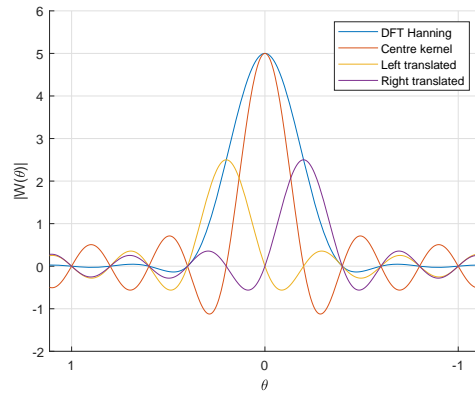


Figure 16: Hanning window in Dirichlet kernels

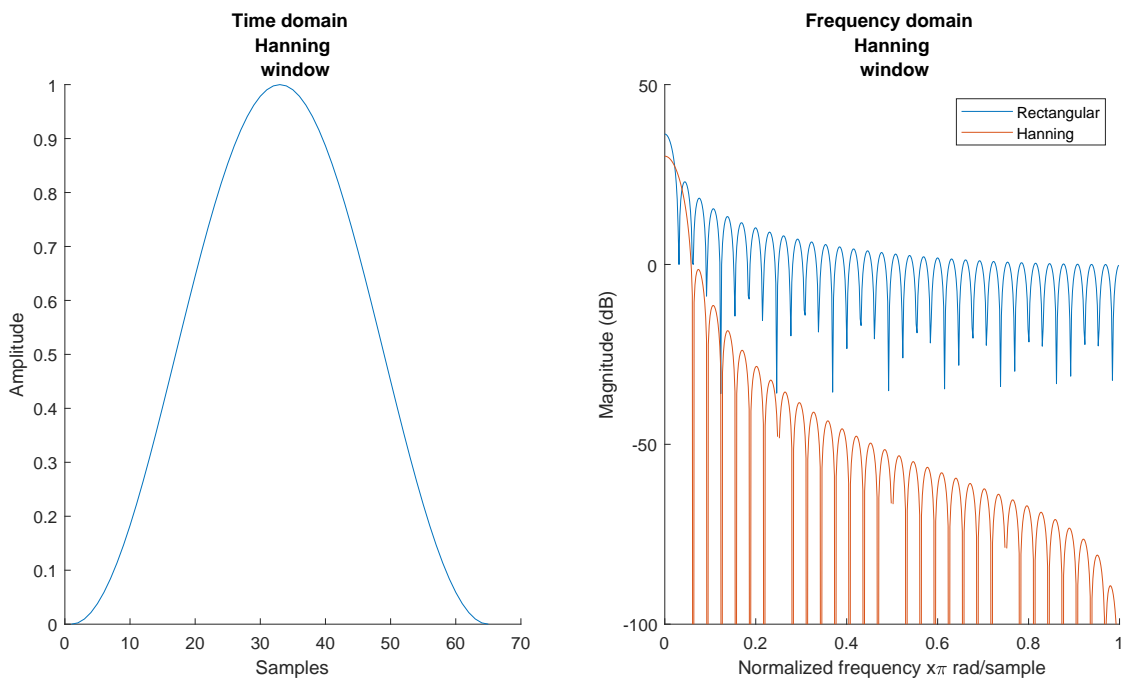


Figure 17: Hanning function in time and frequency domain

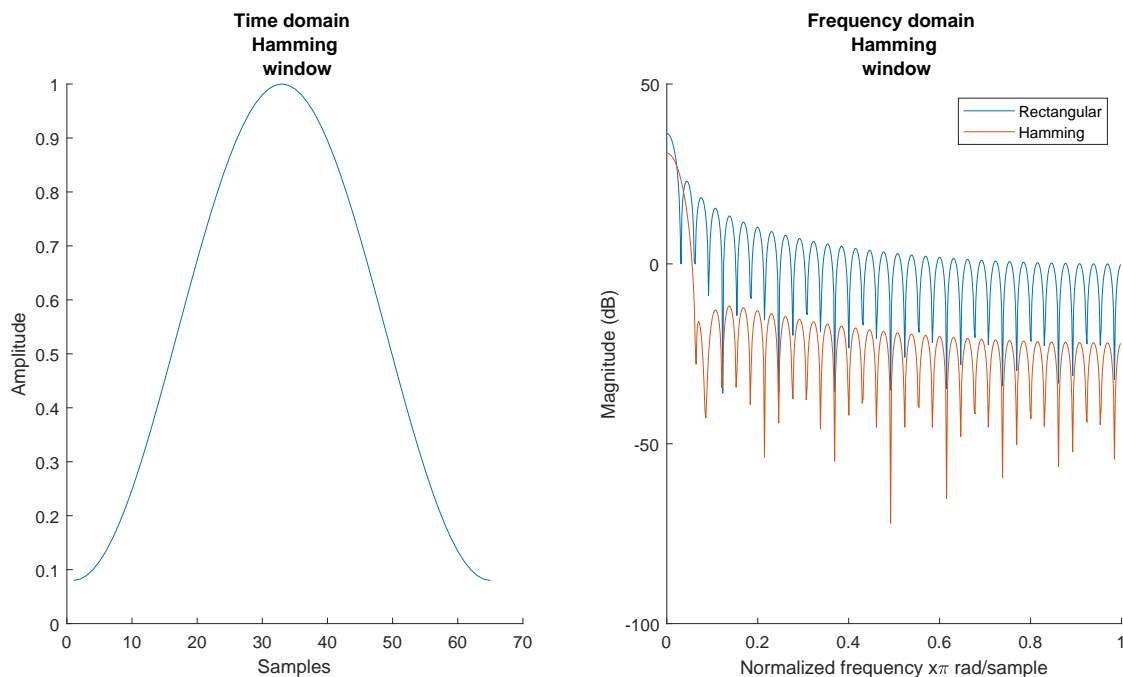


Figure 18: Hamming function in time and frequency domain

If $\alpha = 25/46$ is used, perfect cancellation of the first side lobe is achieved [23].

A.4. Blackman window

The Blackman window is an extension of the Hanning window and it originates from the same function family as the Hanning and the Hamming window. It uses however an extra \cos term to cancel the third and fourth side lobe of the central Dirichlet kernel. This results in a description of the window in equation 34. For a detailed derivation see [24]. The Blackman window can be seen in figure 19.

$$W(n) = 0.42 + 0.5\cos\left[\frac{2\pi}{N}n\right] + 0.08\cos\left[\frac{2\pi}{N}2n\right] \quad (34)$$

A.5. Flat top window

Flat top windows are specifically designed to minimize scalloping losses. The misestimate in amplitude can be 1dB or more depending on the exact conditions and location of the peak with respect to the frequency bins [25]. The goal of flat top windows is to have a response that is as flat as possible in the range $-0.5 \leq f \leq 0.5$. The flattop windows are constructed as a weighted sum of cosines. The flattop window constructed by the matlab

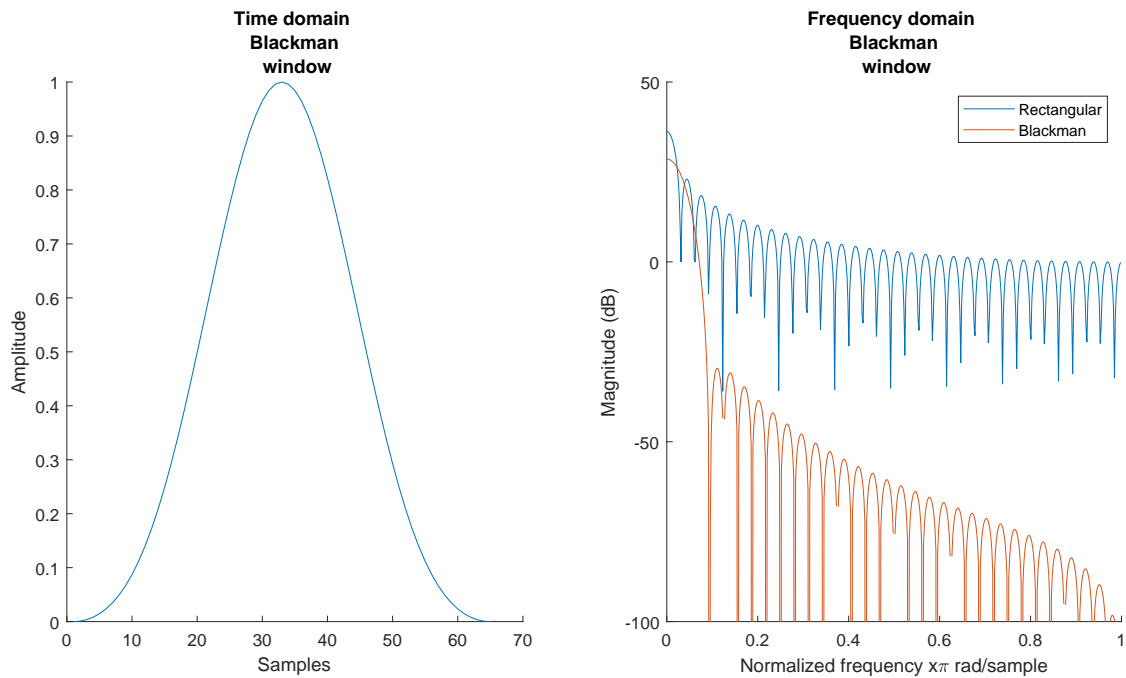


Figure 19: Blackman function in time and frequency domain

Coefficient	Value
a_0	0.215579
a_1	0.416632
a_2	0.277263
a_3	0.083579
a_4	0.006947

Table 1: Flat top window parameters

window design tool is defined as equation 35 in combination with the parameters in table 1. This function is described in [26]. The main disadvantage of the use of this window is the width of the main lobe, which is approximately five times that of the rectangular window [26]. This makes that although the amplitude of the to be measured signal is more accurate than with the previously mentioned window functions, there is in general more leakage. This makes these types of window functions only suitable for the use in specific situations, i.e. calibration [25].

$$w(n) = a_0 - a_1 \cos\left(\frac{2\pi n}{N-1}\right) + a_2 \cos\left(\frac{4\pi n}{N-1}\right) - a_3 \cos\left(\frac{6\pi n}{N-1}\right) + a_4 \cos\left(\frac{8\pi n}{N-1}\right) \quad (35)$$

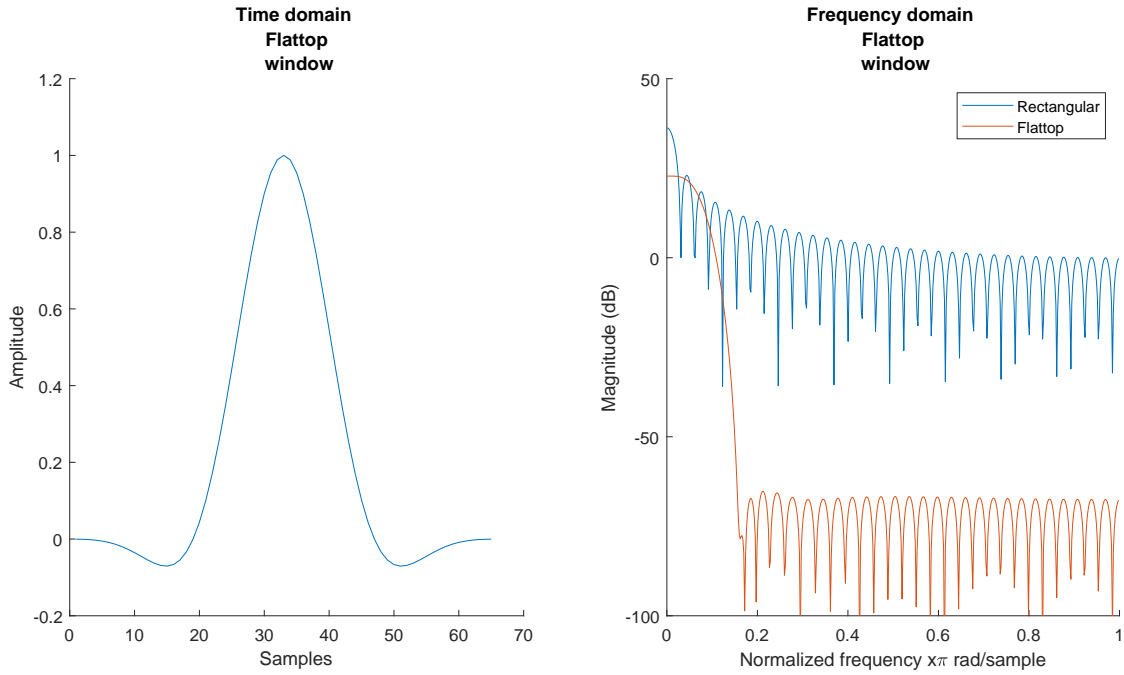


Figure 20: Flattop function in time and frequency domain

A.6. Gaussian window

According to the generalized uncertainty principle, it is impossible to concentrate a time signal and its Fourier transform simultaneously. This means that there always is a trade off between time duration and bandwidth. According to [23], this trade off can be described as equation 36, in which T is the mean squared time duration and W is the mean squared band width. It also states that the only function that can reach the equality is the Gaussian pulse. The Gaussian pulse however extends to infinity, thus to make the function suitable for application as window function the Gaussian pulse needs to be truncated. This results however in a loss of the minimum time-bandwidth property.

$$TW \geq \frac{1}{4\pi} \quad (36)$$

The Gaussian window can be defined by:

$$w(n) = \exp \left[-\frac{1}{2} \left(\alpha \frac{n}{N/2} \right)^2 \right] \quad (37)$$

The parameter α is a measure of the width of the main lobe of the Fourier transform. A high value for α corresponds to a low width of the window. This decreases the severity of the discontinuity introduced at the boundaries of the window due to the truncation of the Gaussian pulse. Note in the frequency domain of the Gaussian pulse that α balances a shallow main lobe with a low side lobe amplitude.

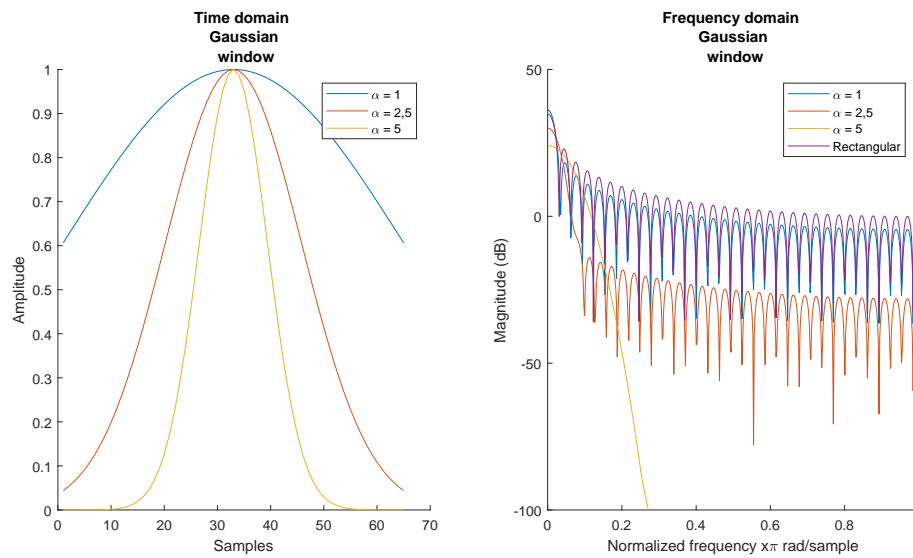


Figure 21: Gaussian function in time and frequency domain

A.7. Kaiser window

The Kaiser window is a restricted time and energy function that maximizes, the energy in a particular band W [23]. The function can be described with equation 38.

$$w(n) = \frac{I_0\left(\pi\alpha\sqrt{1 - \left(\frac{n}{N/2}\right)^2}\right)}{I_0(\pi\alpha)}, \quad 0 \leq |n| \leq \frac{N}{2} \quad (38)$$

With:

$$I_0(X) = \sum_{k=0}^{\infty} \left[\frac{\left(\frac{x}{2}\right)^k}{k!} \right]^2 \quad (39)$$

The function is parametrised with α and the $\pi\alpha$ is half of the time-bandwidth. The Kaiser window can be seen in figure 22.

B. Reflection

At Bosch I functioned as a member of the NVH team and most of the time I spent with experimental evaluation of the eAxle, either in the preparation, the actual experiment or the analysis phase of this process. Most of the time the planning for the experiments would be known about a week in advance, but due to the uncertainties in all enablers of these experiments, like the production, the transport, test bench availability, other

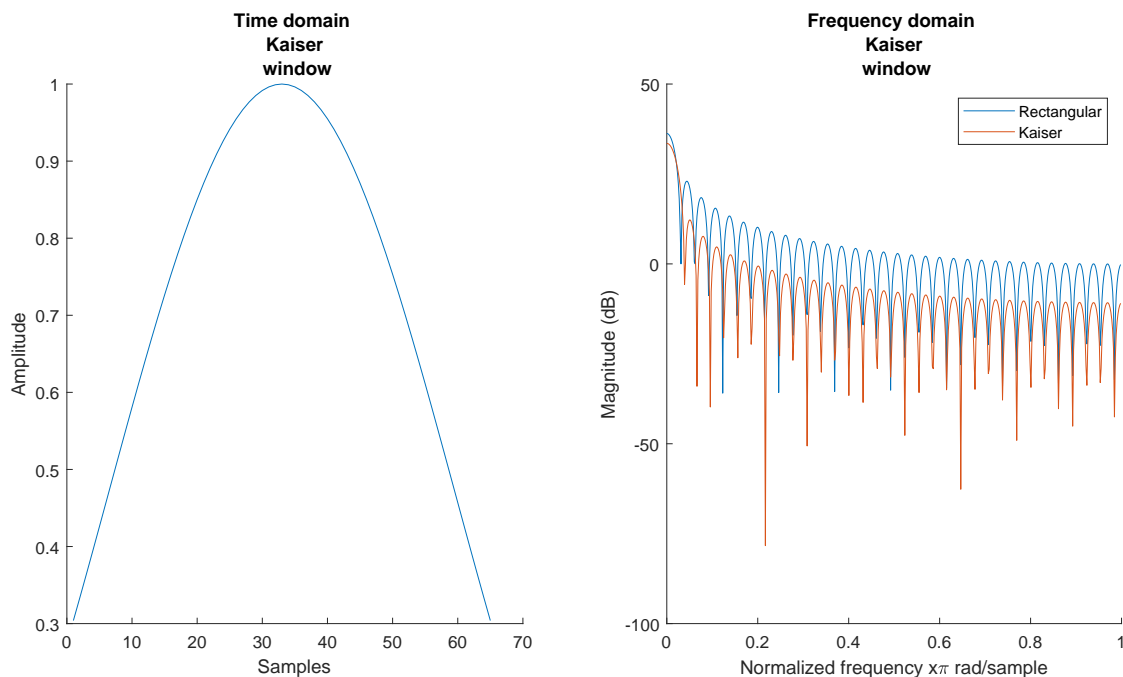


Figure 22: Kaiser function in time and frequency domain

experiments and shifting priorities this planning was highly dynamic. Therefore it could very well happen that when I arrived in the morning there was a message with the request if I could do some measurements asap. This required me to get into contact with many colleagues involved in the process. This was also the case for distributing the results of the experiments over the people interested. All this made that after the some start up problems I really felt a part of the team.

I was also really impressed with the work ethic of the complete team, they were all enthusiastic and motivated to make a good product. Also they were open for questions which allowed me to get quickly up to speed with the project as well as expand my knowledge in other areas of the project.

There were also several other interns in my department and on the Schwieberdingen campus through which I could also come into contact with other projects. Regular after work activities for interns were also organised.

What really suprised me was the availability of resources, either on the Schwieberdingen campus or on other locations. Was a specific type of testbench required for a measurement that was not available in the area then also in the rest of Germany was looked, for example, I visited a testbench in the vicinity of Aachen for 1.5 weeks with a colleague. Also things like borrowing a company car could be organised fast and on short notice.

Altogether I had a very good time at Bosch with my colleagues and fellow students and I learned a lot about functioning in an actual engineering team.

References

- [1] G. Marbjerg, “Noise from electric vehicles - a literature survey,” *Report within Compett project*, 201.
- [2] G. Xie, D. Thompson, and C. Jones, “The radiation efficiency of baffled plates and strips,” *Journal of sound and vibration*, vol. 280, no. 1-2, pp. 181–209, 2005.
- [3] “Bosch homepage.” <https://www.bosch.com/>. Accessed: 10-06-20189.
- [4] “eaxle product page.” <https://www.bosch-mobility-solutions.com/en/products-and-services/passenger-cars-and-light-commercial-vehicles/powertrain-systems/electric-drive/eaxle/>. Accessed: 11-10-2018.
- [5] H. W. Beaty, J. L. Kirtley, N. K. Ghai, R. Lyon, and S. Leeb, *Electric motor handbook*. McGraw-Hill California, 1998.
- [6] W. R. Finley, M. M. Hodowanec, and W. G. Holter, “An analytical approach to solving motor vibration problems,” in *Petroleum and Chemical Industry Conference, 1999. Industry Applications Society 46th Annual*, pp. 217–232, IEEE, 1999.
- [7] S. Lacey, “An overview of bearing vibration analysis,” *Maintenance & asset management*, vol. 23, no. 6, pp. 32–42, 2008.
- [8] N. Akturk, M. Uneeb, and R. Gohar, “The effects of number of balls and preload on vibrations associated with ball bearings,” *Journal of tribology*, vol. 119, no. 4, pp. 747–753, 1997.
- [9] “Tolerances.” <https://www.skf.com/group/products/bearings-units-housings/principles/general-bearing-knowledge/tolerances/index.html>. Accessed: 13-05-2019.
- [10] B. J. Hamrock, S. R. Schmid, and B. O. Jacobson, *Fundamentals of fluid film lubrication*. CRC press, 2004.
- [11] A. Fuchs, E. Nijman, and H.-H. Priebsch, *Automotive NVH Technology*. Springer, 2016.
- [12] J. D. Smith, *Gear noise and vibration*. CRC Press, 2003.
- [13] M. Beghini, F. Presicce, and C. Santus, *A method to define profile modification of spur gear and minimize the transmission error*. AGMA, 2004.
- [14] D. G. Holmes, “A general analytical method for determining the theoretical harmonic components of carrier based pwm strategies,” in *Industry Applications Conference, 1998. Thirty-Third IAS Annual Meeting. The 1998 IEEE*, vol. 2, pp. 1207–1214, IEEE, 1998.

-
- [15] D. G. Holmes and B. P. McGrath, “Opportunities for harmonic cancellation with carrier-based pwm for a two-level and multilevel cascaded inverters,” *IEEE Transactions on industry applications*, vol. 37, no. 2, pp. 574–582, 2001.
- [16] R. J. Allemang, “The modal assurance criterion—twenty years of use and abuse,” *Sound and vibration*, vol. 37, no. 8, pp. 14–23, 2003.
- [17] L. Cremer and M. Heckl, *Structure-borne sound: structural vibrations and sound radiation at audio frequencies*. Springer Science & Business Media, 2013.
- [18] L. Rayleigh, “The theory of sound. mac millan,” 1945.
- [19] F. G. Leppington, E. G. Broadbent, and K. Heron, “The acoustic radiation efficiency of rectangular panels,” *Proceedings of the Royal Society of London. A. Mathematical and Physical Sciences*, vol. 382, no. 1783, pp. 245–271, 1982.
- [20] B. J. Schwarz and M. H. Richardson, “Experimental modal analysis,” *CSI Reliability week*, vol. 35, no. 1, pp. 1–12, 1999.
- [21] L. Ljung, “System identification: theory for the user. 1987 prentice-hall englewood cliffs,” 1987.
- [22] R. D. Cook, D. S. Malkus, M. E. Plesha, and R. J. Witt, *Concepts and applications of finite element analysis*, vol. 4. Wiley New York, 1974.
- [23] F. J. Harris, “On the use of windows for harmonic analysis with the discrete fourier transform,” *Proceedings of the IEEE*, vol. 66, no. 1, pp. 51–83, 1978.
- [24] A. Dale, “Gear noise and the sideband phenomenon,” *ASME Paper*, vol. 84, 1984.
- [25] G. Heinzel, A. Rüdiger, and R. Schilling, “Spectrum and spectral density estimation by the discrete fourier transform (dft), including a comprehensive list of window functions and some new at-top windows,” 2002.
- [26] G. D’Antona and A. Ferrero, *Digital signal processing for measurement systems: theory and applications*. Springer Science & Business Media, 2005.